

Nonequilibrium breakdown of a correlated insulator through pattern formationPedro Ribeiro,^{1,2} Andrey E. Antipov,³ and Alexey N. Rubtsov^{1,4}¹*Russian Quantum Center, Novaya Street 100 A, Skolkovo, Moscow Area 143025, Russia*²*CeFEMA, Instituto Superior Técnico, Universidade de Lisboa Av. Rovisco Pais, 1049-001 Lisboa, Portugal*³*Department of Physics, University of Michigan, Randall Laboratory, 450 Church Street, Ann Arbor, Michigan 48109-1040, USA*⁴*Department of Physics, Lomonosov Moscow State University, Leninskie gory 1, 119991 Moscow, Russia*

(Received 17 February 2016; revised manuscript received 5 April 2016; published 25 April 2016)

We study the breakdown of an interaction-induced insulator under an imposed bias voltage. A rich voltage-temperature phase diagram is found that contains phases with a spatially patterned charge gap. Nonequilibrium conditions are shown to be able to change the antiferromagnetic nature of the equilibrium correlations. Above a threshold voltage, smaller than the charge gap, the formation of patterns occurs together with the emergence of midgap states yielding a finite conductance. We discuss the experimental implications of this proposed scenario for the breakdown of the insulating state.

DOI: [10.1103/PhysRevB.93.144305](https://doi.org/10.1103/PhysRevB.93.144305)**I. INTRODUCTION**

Pattern formation, known also as self-organization, refers to the occurrence of spatial-structured steady states in nonlinear systems under out-of-equilibrium external conditions [1]. A textbook illustration is the Rayleigh-Bénard convection, but examples are found ubiquitously in physical, chemical, as well as biological systems [2,3].

In semiconductors, pattern formation is a hallmark of voltage-driven nonequilibrium phase transition from insulating to metallic states [4]. Moving patterns that arise near phase boundaries contribute to a finite conductivity. These phenomena can essentially be explained neglecting electron-electron interactions. A seminal experiment, revealing pattern formation in strongly correlated materials [5], reported current-induced patterns in a quasi-one-dimensional organic charge-transfer complex on the verge of Mott breakdown. The reported nonlinear I - V characteristic shows an intermediate-voltage low-resistance state characterized by a striped charge pattern, before the switching to a metallic regime. Recently, experimental results for spinor Bose-Einstein condensates [6] and theoretical studies of polariton condensates [7,8] also reported patterned phases.

Nonequilibrium dynamics of strongly correlated quantum systems has been receiving an increasing amount of attention due to a rich interplay between electronic kinetics, interaction, and nonequilibrium conditions. Major experimental progress was driven forward by a tight control of the dynamics in cold atomic setups [9–11] and pump-probe experiments [12,13]. On the theory side, substantial progress has been made in understanding thermalization and dissipation [14–17], as well as universal aspects of nonequilibrium phase transitions [18–26]. Further developments also arose concerning novel computational methods [27–31] and techniques [32–34]. In particular, the study of out-of-equilibrium properties of the Hubbard model has been an active research area [32,35–42]. Interesting dynamical transitions between small and large interaction quenches were shown to occur at half-filling [33,34,43–45]. Transport properties at finite temperature [46] and in the presence of Markovian [47,48] and non Markovian [49,50] dissipation have also been recently investigated.

A key problem is the understanding of the transition from an interaction-induced insulator to a current-carrying state upon increasing the bias voltage applied by external leads. The generated electrochemical gradients induce two effects of a rather different nature: (i) a thermodynamic imbalance depending on the electronic distribution functions in the leads, and (ii) the coupling of charged particles to the electric field created by the voltage drop. The breakdown of a Mott insulator induced by effect (ii) recently received important contributions. Using the Peierls substitution argument, (ii) can be studied on a system with periodic boundary conditions pierced by a linear-in-time magnetic flux. The procedure eliminates the need for an explicit treatment of the reservoirs and renders the problem amenable to Lanczos [51], the density-matrix renormalization group (DMRG) [52], dynamical mean-field theory (DMFT) [40,53–56], nonequilibrium Green's functions [57], and analytic [58,59] methods. These studies revealed a qualitative scenario that can be interpreted as the many-body analog of the Landau-Zener (LZ) mechanism observed in band insulators [51]: the LZ energy scale sets a threshold $V_{\text{th}} \sim \Delta^2 L/W$ above which a field-induced metallic phase sets in, with Δ the charge gap, L the system's linear size, and W the bandwidth. Zener's formula yields $V_{\text{th}}/L \gg \Delta$, overestimating experimentally measured values of threshold fields [60–62].

The combined effect of (i) and (ii), which requires an explicit treatment of the reservoirs, has been recently addressed using nonequilibrium Green's function approaches [63,64] and within the framework of time-dependent density-matrix renormalization-group (tDMRG) methods [65]. Both sets of results are compatible with a current-voltage characteristics of the form $J \simeq V e^{-V_{\text{th}}/V}$. A thorough study [64], assuming antiferromagnetic correlations and carried out at $T = 0$ in the presence of long-range Coulomb interactions, pointed out that the dominant effect depends on the ratio between the correlation length in the insulating phase ξ and the size of the insulating region L . For $\xi/L \gg 1$, (i) leads to $V_{\text{th}} \sim \Delta$; for $\xi/L \ll 1$, (ii) dominates and the LZ scenario is recovered.

In previous studies, the assumption that antiferromagnetic correlations prevail has precluded the prediction of any pattern formation. Relaxing this assumption, we are able to address the existence of patterned states in strongly correlated electronic

systems under nonequilibrium conditions. Here, the half-filled Hubbard model is considered, where the equilibrium low-temperature state is an insulator due to electron-electron interactions. We address the out-of-equilibrium properties of a Hubbard chain coupled to metallic leads held at different chemical potentials. We focus on thermodynamic-imbalance effects, dubbed (i) in the previous discussion. The presence of the leads induces the nonequilibrium conditions and provides an intrinsically non-Markovian [50] dissipative environment ensuring that a steady-state solution exists for asymptotically large times at the mean-field level. We compute the instabilities of the system to spatially modulated patterns, identify a rich set of candidate phases (among which are examples of pattern formation), and analyze their properties in the nonlinear regime. Nonequilibrium conditions are shown to change the underlying correlations of the equilibrium state. We put forward a scenario for the breakdown of an interaction-induced insulating phase through the emergence of conducting midgap states that coincides with the appearance of patterns for $V_{\text{th}} \lesssim \Delta$. Our results are of direct relevance to interpret the properties of quasi-one-dimensional organic compounds [5] where pattern formation has been reported.

II. MODEL AND METHODS

We consider the interacting system S, depicted in Fig. 1(a), consisting of a chain coupled to metallic reservoirs. The Hamiltonian can be decomposed as $H = H_S + H_{\partial S} + H_{\bar{S}}$, where

$$H_S = -t \sum_{(r,r'),s} c_{r,s}^\dagger c_{r',s} + \frac{U}{2} \sum_r (n_r - 1)^2 \quad (1)$$

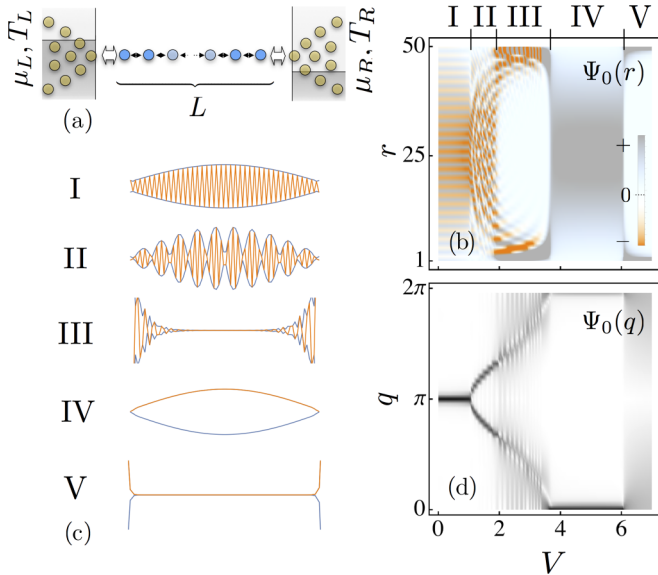


FIG. 1. (a) Schematic view of the physical setup. (b) Density plot of the first unstable mode $\Psi_0(r)$ plotted as a function of the bias V for $\Gamma = 0.25$, $T = 0.25$, $L = 50$, and for $U = U_c(T, V)$. The phase labels I, \dots, V point to qualitatively different behavior of $\Psi_0(r)$. (c) Typical spatial dependence of $\Psi_0(r)$ in each phase (orange line), plotted for $L = 80$. The blue line depicts the envelope function. (d) Density plot of the Fourier transform $\Psi_0(q)$ of $\Psi_0(r)$ as a function of q computed for $L = 50$.

is the Hamiltonian of the system, consisting of a fermionic Hubbard chain, with s labeling spin degrees of freedom and $n_r = \sum_s c_{r,s}^\dagger c_{r,s}$. The hopping matrix element between nearest-neighbor sites is taken to be the energy unit, i.e., $t = 1$. $H_{\bar{S}} = \sum_{\alpha,s,l} d_{l\alpha s}^\dagger \epsilon_{l,\alpha} d_{l\alpha s}$ is the Hamiltonian of the reservoirs, with $l = L, R$ labeling the reservoir and α the reservoir's single-particle modes. The density of states of the leads is taken to be that of a wide-band metal, i.e., constant within all the relevant energy scales. The system-reservoir coupling is described by the hopping term $H_{\partial S} = \sum_{\alpha,s,l} v d_{l\alpha s}^\dagger c_{r_1,s} + \text{H.c.}$, where $r_{L,R}$ are the sites at the extremities of the chain and v is the hopping amplitude. Under these assumptions, the reservoirs are characterized solely by their hybridization constant $\Gamma = \pi v^2 \rho$, with ρ the reservoir's density of states, and by their thermodynamic potentials: temperature T_l and chemical potential μ_l . We take $T = T_R = T_L$ and $\mu_L = -\mu_R = V/2$, with V the applied bias voltage. For simplicity, Γ is assumed to be the same for both reservoirs.

In the following, we employ a nonequilibrium mean-field approach to study the effects of the applied voltage. In equilibrium, the mean-field treatment overestimates the role of correlations that may lead to the prediction of ordered states in one-dimensional systems, whereas phases that break a continuous symmetry are forbidden by the Mermin-Wagner theorem. For the one-dimensional half-filled Hubbard model, mean field predicts an antiferromagnetic state whereas the ground state is disordered with slowly (algebraic) decaying antiferromagnetic correlations. Charge properties, featuring an insulating state with a finite charge gap, are quantitatively reproduced for small and intermediate U . The ordered state, therefore, captures the most prominent correlations of the paramagnetic ground state and recovers the charge properties for small U . Out of equilibrium, the mean-field treatment is also expected to overestimate the role of correlations, and its results must still be taken at a qualitative level. Nonetheless, it should provide a clear physical picture of the underlying physics.

The procedure to obtain the mean-field equations and the magnetic susceptibility is standard and is given in Appendices A and B for completeness. Here we outline the main steps. Working on the Keldysh contour, we use the identity [66]

$$\frac{U}{2} (n_r - 1)^2 = -\frac{U}{3} \mathbf{S}_r \cdot \mathbf{S}_r + \frac{U}{4} (n_r - 1)^2 + \frac{U}{4}, \quad (2)$$

with $\mathbf{S}_r = \frac{1}{2} c_{r,s}^\dagger \boldsymbol{\sigma}_{ss'} c_{r,s'}$. Equation (2) is valid for fermionic and Grassmanian fields and does not introduce any renormalization of the chemical potential. A three-component Hubbard-Stratonovich field $\boldsymbol{\phi}$ and a scalar field ϱ are introduced to decouple the interaction term in the spin-density-wave channel $\frac{U}{3} \mathbf{S}_r \cdot \mathbf{S}_r \rightarrow \mathbf{S}_r \cdot \boldsymbol{\phi}_r + \frac{1}{2} \frac{3}{2U} \boldsymbol{\phi}_r \cdot \boldsymbol{\phi}_r$ and in the charge-density channel $\frac{U}{4} (n_r - 1)^2 \rightarrow (n_r - 1) \cdot \varrho_r + \frac{1}{2} \frac{1}{2U} \varrho_r \cdot \varrho_r$. Note that ϱ_r corresponds to local deviations with respect to half-filling. Assuming a wide-band limit, the integration of the noninteracting reservoirs yields a local self-energy contribution to the c electrons (see Appendix A 2): $\Sigma_{r=r_1, r'=r_1}^{R/A}(t, t') \simeq \mp i \Gamma \delta(t - t')$, $\Sigma_{r=r_1, r'=r_1}^K(t, t') \simeq -2i \Gamma \int \frac{d\varepsilon}{2\pi} \tanh[\frac{\beta \varepsilon}{2} (\varepsilon - \mu_l)] e^{-i\varepsilon(t-t')}$. Finally, integrating out the c degrees

of freedom, we arrive at an action uniquely dependent on the fields ϕ and ϱ . We use the Keldysh rotation of the time-dependent order parameter to its quantum and classical components ($\phi_{c,r}, \phi_{q,r}$), and by varying the action with respect to these fields, we obtain a set of saddle-point equations with $\phi_{q,r}(t) = \varrho_{q,r}(t) = 0$. We focus on the steady-state regime and parametrize the classical component of steady-state solutions by

$$\phi_{c,r}(t) = \sqrt{2}\phi_r, \quad (3)$$

$$\varrho_{c,r}(t) = i2\sqrt{2}\mu_r, \quad (4)$$

anticipating that ϱ has an imaginary stationary solution. In these variables, the mean-field self-consistent conditions are given by

$$\phi_r = -i\frac{U}{3}\text{tr}\left[G_{rr}^K(t,t)\frac{\sigma}{2}\right], \quad (5)$$

$$\mu_r = -i\frac{U}{2}\text{tr}\left[G_{rr}^K(t,t)\frac{1}{2}\right], \quad (6)$$

where $G_{rr}^K(t,t)$ is the Keldysh component of the local c -electron Green's function. At the mean-field level, the excitation spectrum is given by the non-Hermitian mean-field operator

$$K = -t \sum_{(r,r'),s} c_{rs}^\dagger c_{r's} - i\Gamma \sum_{l,s} c_{rls}^\dagger c_{rls} + \sum_{rs'} \left(-\frac{1}{2} \sigma_{ss'} \cdot \phi_{r'} - \mu_{r'} \right) c_{rs}^\dagger c_{rs'}. \quad (7)$$

The retarded Green's function is obtained in terms of the left ($|\tilde{\alpha}\rangle$) and right ($|\alpha\rangle$) eigenvectors of K with complex eigenvalues λ_α ($\text{Im}\lambda_\alpha < 0$): $G^R(\omega) = \sum_\alpha |\alpha\rangle(\omega - \lambda_\alpha)^{-1}\langle\tilde{\alpha}|$. The Keldysh component, derived in detail in Appendix B 2, is obtained in a similar way.

Within the mean-field approximation, there is a unique steady state for a given spin-density-wave profile ϕ_r . This result follows from the uniqueness of the steady state for noninteracting systems in the absence of bound states [67], here ensured by the presence of the wide-band leads [50]. For interacting open systems with a few degrees of freedom, a unique steady state has also been generically found [68–70]. Together these two facts strongly suggest the existence of a unique steady state in the present case, at least for finite chains.

Fluctuations around the mean field further provide a stability analysis for the saddle-point solutions. To investigate the possible steady states that can be realized under nonequilibrium conditions, we compute the spin susceptibility χ in the disordered state ($\phi_r = 0$) and analyze the first unstable modes arising upon increasing U . The retarded spin susceptibility $\chi_{ii',rr'}^R(t,t') = -i\Theta(t-t')\langle\{S_r^i(t), S_{r'}^{i'}(t')\}\rangle$ (with $i, i' = x, y, z$) is given by the random-phase approximation (RPA) -type expression, which, in the steady state, reads

$$[\chi_{ii'}^R(\omega)]_{rr'}^{-1} = \frac{1}{2}\delta_{ii'} \left[-\frac{3}{U}\delta_{rr'} - \Xi_{rr'}^R(\omega) \right], \quad (8)$$

where $\Xi_{rr'}^R(t,t') = -i\frac{1}{2}\text{tr}[G_{rr'}^A(t',t)G_{rr'}^K(t,t') + G_{rr'}^K(t',t)G_{rr'}^R(t,t')]$ is the bare bubble diagram computed at $\phi_r, \varrho_r = 0$,

and $G_{rr'}^{R/A}(t,t')$ are the spatially resolved retarded/advanced components of the Green's function of the c electrons.

Upon increasing U , the eigenvalues of $\chi^R(\omega)$ as a function of ω may develop poles in the upper-half of the complex plane. When this occurs, small perturbations in the direction of the corresponding eigenmode of $\chi^R(\omega)$ grow exponentially in time until anharmonic mode-coupling terms start to be relevant. This process signals an instability of the system. In the linear regime, for U sufficiently close to U_c , the new stable phase, arising for $U > U_c$, is expected to develop the spatial structure of the lowest eigenmode of $\chi^R(\omega)$. In the following, we assume that unstable modes first occur for steady-state solutions, i.e., at $\omega = 0$. The unstable mode corresponds to the most negative eigenvalue λ_0^Ξ of $\Xi^R(\omega = 0)$, and its spatial configuration is given by the corresponding eigenvector $\Psi_0(r)$.

In an equilibrium setup, where the system is assumed to be in a Gibbs state with density matrix $\rho = e^{-\beta(H-\mu N)}/Z$, periodic boundary conditions lead to $\Psi_0(r) = \frac{1}{\sqrt{L}}e^{iQr}$, with $Q = \pi$ signaling an instability toward the antiferromagnetically ordered phase. This picture is essentially unchanged in the presence of open boundary conditions with the order parameter amplitude typically getting distorted near the boundaries of the system. Note that for $V = 0$, the presence of the leads with a finite hybridization Γ does not change this scenario, and in the limit $\Gamma \rightarrow 0^+$ the equilibrium Gibbs state is recovered in the steady state.

III. RESULTS

To ensure half-filling, we set the $\mu_L = -\mu_R = V/2$. With this prescription, all the obtained self-consistent solutions of μ_r were found to vanish, therefore in the following we set $\mu_r = 0$ and focus only on ϕ_r . Figures 1(b) and 1(c) depict the typical spatial structure of steady state $\Psi_0(r)$ obtained upon varying the bias voltage V . Five different phases (labeled by I, \dots, V) can be observed, corresponding to qualitatively different features of $\Psi_0(r)$. Figure 1(d) depicts a contour plot of the Fourier transform $\Psi_0(q)$ of $\Psi_0(r)$ showing that the different phases correspond to different wave vectors Q for which $|\Psi_0(Q)|$ is maximal. Phase I occurs for low voltages $V < V_{\text{AF}}$ and $T > 0$ and occupies a region where the antiferromagnetic phase corresponds to the first instability. The order parameter is maximal in the center of the system. The emergence of patterns is visible in phase II ($V_{\text{AF}} < V < V_{\text{loc}}$), where the spin-susceptibility instability corresponds to an ordered state with wave vectors $q = \pm Q$, with Q varying continuously from its antiferromagnetic value π , for $V = V_{\text{AF}}$, to a new value $Q \leq 0$, for $V = V_{\text{loc}}$. Phase III ($V_{\text{loc}} < V < V_{\text{F}}$) corresponds to a modulated phase, with $Q \neq 0, \pi$, exponentially localized near the leads. Phase IV ($V_{\text{F}} < V < V_0$) is a ferromagnetic phase with an envelope function that is maximal at the center of the system. Finally, phase V corresponds to an essentially disordered phase ($\phi = 0$) with the order-parameter amplitude being localized in the first few sites near the leads.

Figure 2(a) shows the phase diagram in the V - T plane for $\Gamma = 0.25$ near $U = U_c(T, V)$ for which the first instability arises. Other values of Γ within the range 0.05–0.5 yield qualitatively similar results. At $T = 0$, the antiferromagnetism of phase I is unstable under any finite bias voltage giving place

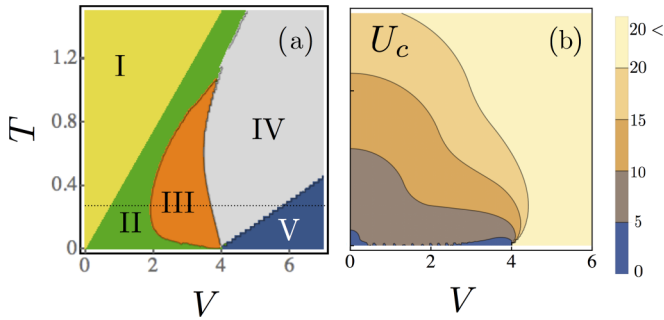


FIG. 2. (a) Phase diagram as a function of V and T for $U = U_c(T, V)$, corresponding to the appearance of the first unstable mode, computed for $\Gamma = 0.25$. The dashed line corresponds to Figs. 1(b) and 1(c). (b) Values of U_c for which the first instability arises as a function of V and T , for $\Gamma = 0.25$ and $L = 50$.

to the modulated phase II. Moreover, at zero temperature no ferromagnetic phase is present yielding a direct transition from II to the disordered phase V. The localized modulated phase III is present only for intermediate temperatures. For sufficiently high temperatures, within the range of temperatures and voltages studied, only phases I, II, and IV are observed. The critical value of U , given by $U_c = -3/\lambda_0^{\Xi}$ after Eq. (8), is plotted in Fig. 2(b) for a system with $L = 50$. For low temperature, this quantity is subjected to strong finite-size corrections for small U . Care must be taken extrapolating to the thermodynamic limit, nonetheless we verify that for $T \rightarrow 0$ and $L \rightarrow \infty$ one has $U_c \rightarrow 0$ (see Appendix D).

To verify the existence of well-defined patterns at $U \gg U_c$ and to describe their spatial structure, the linear-response RPA-type description is insufficient, as nonlinear terms in Eq. (5) start to play an important role and have to be taken into account. In this regime, the mean-field solution for the order parameter ϕ is obtained solving the self-consistent relation in Eq. (5). The procedure is done iteratively allowing only for collinear magnetized states, i.e., $\langle \mathcal{S}_r \rangle \propto \hat{e}_z$. Figure 3(a) shows the spatial structure of ϕ_r obtained in this way. The considered value of $U = 6.3$ corresponds to an equilibrium ($V = 0$) charge gap of $\Delta = 2|\phi| \simeq 1.57$. Out of equilibrium, phases III–V are absent, and the range of values of V for which phase II arises is reduced with respect to the diagram of Fig. 2(a). Nevertheless, a modulated solution can be found deep in the nonlinear regime. Figure 3(b) depicts the maximum value of the order-parameter amplitude ϕ_{Max} showing that phase II transits directly to the disordered phase $\phi = 0$ upon increasing V .

Figure 3(b) shows also the values of the particle current through the system. A relatively low current in phase I is followed by a quick rise of current during phase II and a linear I - V characteristics in the disordered phase. Figures 3(c)–3(e.1) show the integrated steady-state density of states in phase II. One observes that upon increasing V , a new band of conducting states arises, corresponding to single-particle energies $-V/2 < \text{Re}\lambda_\alpha < V/2$. The appearance of such states is responsible for the current increase in phase II. This phase ceases to exist when V becomes of the order of the interband gap, roughly given by ϕ_{Max} , corresponding to a complete filling of the gap by conducting states. The I - V characteristics can

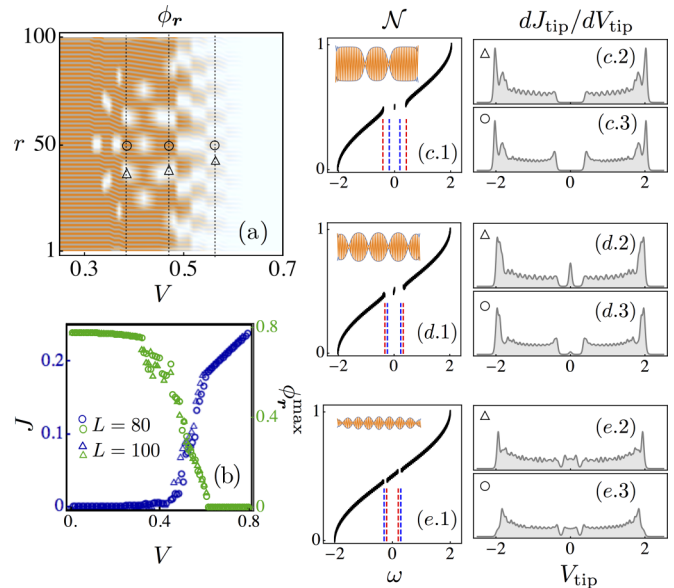


FIG. 3. Properties for $U > U_c$ obtained for $\Gamma = 0.25$, $T = 0.03$, and $U = 6.3$ corresponding to an equilibrium ($V = 0$) charge gap of $\Delta = 2|\phi| \simeq 1.57$. (a) Density plot of $\Phi(r)$ plotted as a function of V for $L = 100$. The lines and markers label the specific values of (c)–(e). (b) Maximum value of the order parameter $\phi_{\text{Max}} = \max_r |\phi_r|$ (green) and particle current through the chain J (blue) as a function of V for $L = 80$ (circles) and $L = 100$ (triangles). (c.1) Integrated density of states $\mathcal{N}(\omega) = \sum_\alpha \Theta(\omega - \text{Re}\lambda_\alpha)$ for $V = 0.38$ and $L = 100$; the thickness of the black line is given by $\text{Im}\lambda_\alpha$. The red dashed lines correspond to $\omega = \pm\Phi_{\text{Max}}$ and the blue dashed lines to $\omega = \pm V/2$. The inset depicts the spatial dependence of $\phi(r)$. (c.2), (c.3) Differential conductance $dJ_{\text{tip}}/dV_{\text{tip}}$ obtained by an STM tip, computed for $T_{\text{tip}} = 0.02$, placed at position r , for $r = 37$ (c.2) and $r = 50$ (c.3), corresponding to a minimum and a maximum of the order-parameter amplitude. (d.1)–(d.3) Same as (c.1)–(c.3) for $V = 0.48$, $r = 40$, and $r = 50$. (e.1)–(e.3) Same as (c.1)–(c.3) for $V = 0.58$, $r = 44$, and $r = 50$.

thus be used as a diagnostic to discriminate between different phases.

The spatially dependent amplitude of the antiferromagnetic order parameter corresponds to a spin- and site-modulated potential seen by the electrons. In the patterned phase, the regions near the nodes of the order parameter form well-like regions that low-energy electrons can occupy. Midgap states can thus be seen as Bloch waves of low-energy electrons whose wave function is maximal in the regions where the order-parameter amplitude vanishes.

To further characterize these states, we monitor the differential conductivity that is measured by a scanning tunneling microscope (STM) tip placed over site r . Assuming a wide-band metallic tip with constant density of states (DOS), weakly coupled to the chain at position r , one obtains the standard linear-response expression

$$\frac{dJ_{\text{tip}}}{dV_{\text{tip}}} \propto - \int d\omega \frac{\beta_{\text{tip}}/2}{\cosh[\beta_{\text{tip}}(\omega - V_{\text{tip}})] + 1} \rho_r(\omega),$$

where $\rho_r(\omega) = \text{tr}[G_{r,r}^R(\omega) - G_{r,r}^A(\omega)]/(-2\pi i)$ is the local DOS of the chain at site r , and β_{tip} and V_{tip} are, respectively, the tip's inverse temperature and chemical potential.

Figures 3(c.2), 3(c.3), 3(e.2), and 3(e.3) show $dJ_{\text{tip}}/dV_{\text{tip}}$ for sites corresponding to minima and maxima of the order parameter for three values of V within phase II. The band of conducting states can clearly be seen arising within the gap. The local DOS for $|V_{\text{tip}}| < \phi_{\text{Max}}$ increases or decreases, depending on whether a position corresponding to a minimum or a maximum of the order-parameter amplitude is monitored.

IV. DISCUSSION

To summarize, we have described a scenario for the breakdown of an interaction-induced insulator through pattern formation in a correlated electronic system under strong nonequilibrium conditions imposed by a finite bias voltage. The development of a conducting phase occurs at voltages smaller than the value of the charge gap and is characterized by the emergence of the midgap states. The thermodynamic imbalance imposed by a finite applied voltage generates a rich set of novel behaviors, among which are examples of nonequilibrium spatially induced patterned phases. Such phases, well studied in classical systems, and recently predicted in systems with Markovian dissipation [7,8], are reported here for the fermionic Hubbard model with a non-Markovian environment and shown to exist down to zero temperature. The suggested mechanism can be tested experimentally monitoring current transport across the system and by STM measurements, spatially resolving the modulated charge gap.

Note that, strictly in one dimension, the phase transitions obtained at the mean-field level should instead correspond to crossovers. In the same way, the calculated magnetic order likely corresponds to a disordered phase with slow power-law decaying spin-spin correlation functions with a voltage-dependent momentum. Nonetheless, charge properties should be qualitatively captured.

The presence of a dissipative environment, other than the leads, acting extensively throughout the system may help to stabilize the magnetic order, seen at the mean-field level. In this case, our results can be used to qualitatively predict magnetic properties in addition to charge ones. The emergent order can otherwise be stabilized in quasi-one-dimensional systems of weakly coupled chains. These considerations capture characteristic features of the breakdown of the organic charge insulator, reported in Ref. [5]. There, upon increasing voltage, the authors observed the presence of an intermediate resistance regime between an insulating and a metallic phase with an I - V characteristic similar to that of Fig. 2(b). Charge-coupled-device (CCD) imaging of the intermediate phase revealed spatially separated regions of alternating concentrations of low-energy charge carriers, not present either in the insulating or in the metallic phase. Important differences, such as a diffusive electronic transport and the long-range Coulomb interactions within the insulating phase, hinder a quantitative prediction of experimental observations.

The present results suggest that, as in the case of classical systems, patterned phases can be ubiquitous in the presence of interactions and spatially nonuniform out-of-equilibrium conditions. In particular, for electronic systems with $d > 1$, pattern formation can be predicted by our method and may help to shed light on spatial structures observed near the dielectric breakdown of certain Mott compounds [61,62]. In

films and bulk compounds, these effects should depend on the orientation of the nonequilibrium drive with respect to the Fermi surface, opening possibilities for novel patterned phases. Nonequilibrium phase transitions to patterned phases, in particular at zero temperature where quantum effects are most relevant, present an interesting paradigm in which new universal behavior could be found.

ACKNOWLEDGMENTS

That authors acknowledge J. P. F. LeBlanc and V. R. Vieira for fruitful discussions. A.E.A. is supported by DOE Grant No. ER 46932. A.E.A. acknowledges the Russian Quantum Center for hospitality. P.R. acknowledges financial support from Fundação para a Ciência e a Tecnologia (Portugal) through Contract No. IF/00347/2014/CP1214/CT0002 under the IF2014 program.

APPENDIX A: KELDYSH ACTION

1. Generating functional

The generating function in the Keldysh contour γ is defined as

$$Z = \int DC e^{i[C^\dagger g^{-1} C] - i \int_\gamma dz \frac{U}{2} \sum_r [n_r(z) - 1]^2}, \quad (\text{A1})$$

where $C = (c \ d_L \ d_R)^T$, and

$$g^{-1} = \begin{pmatrix} g_\Sigma^{-1} & -V_L & -V_R \\ -V_L^\dagger & g_L^{-1} & 0 \\ -V_R^\dagger & 0 & g_R^{-1} \end{pmatrix} \quad (\text{A2})$$

is the inverse of the bare Green's function with

$$g_{S;r,r'}^{-1}(z,z') = \delta(z-z')(\delta_{r,r'} i \partial_z + \tilde{\mathbf{t}}_{r,r'}), \quad (\text{A3})$$

$$g_{l;\alpha,\alpha'}^{-1} = \delta_{\alpha,\alpha'} \delta(z-z')(i \partial_z - \epsilon_{l,\alpha}), \quad (\text{A4})$$

$$V_{l;r,\alpha} = v_l \delta_{r,r_l}. \quad (\text{A5})$$

After using the identity in Eq. (2) and inserting a vectorial 3-component Hubbard-Stratonovich ϕ and a scalar field ϱ to decouple the interactions, one obtains, by integrating out the electronic degrees of freedom, $Z = \int D\phi e^{iS[\phi]}$, where

$$S[\phi] = \frac{1}{2} \sum_r \int_\gamma dz \pi_i^{-1} \phi_r^i(z) \cdot \phi_r^i(z) - \frac{i}{2} \int_\gamma dz \sum_r \varrho_r + \frac{1}{2} \sum_r \int_\gamma dz \pi_0^{-1} \varrho_r^2(z) - i \text{tr} \ln[-iG^{-1}], \quad (\text{A6})$$

with $\pi_{x,y,z}^{-1} = -\frac{3}{2U}$ and $\pi_0^{-1} = -\frac{1}{2U}$, and G given by Dyson's equation:

$$G^{-1} = g_S^{-1} - \Sigma_L - \Sigma_R - \Sigma_\phi, \quad (\text{A7})$$

where

$$\Sigma_{l;r,r'}(z,z') = |v_l|^2 \sum_\alpha g_{l;\alpha,\alpha}(z,z') \delta_{r,r_l} \delta_{r',r_l}, \quad (\text{A8})$$

$$\Sigma_{\phi;r,r'} = -\frac{1}{2} [\boldsymbol{\sigma} \cdot \boldsymbol{\phi}_r(z) + i \varrho_r(z)] \delta_{r,r'} \delta(z-z'). \quad (\text{A9})$$

2. Properties of the reservoirs

As mentioned in the main text, the reservoirs are assumed to be metallic leads with a constant density of states within all relevant energy scales. The reservoirs are also considered to be infinite and are held in a thermal state characterized by a chemical potential μ_l and a temperature T_l . Under these assumptions, we can write

$$\Sigma_l^{R/A}(t, t') \simeq \mp i \Gamma_l \delta(t - t') |\mathbf{r}_l\rangle \langle \mathbf{r}_l|, \quad (\text{A10})$$

$$\Sigma_l^K(t, t') \simeq -2i \Gamma_l F_l(t - t') |\mathbf{r}_l\rangle \langle \mathbf{r}_l|, \quad (\text{A11})$$

with $\Gamma_l = \pi |v_l|^2 \rho_l(0)$, with $\rho_l(0)$ the density of states of the reservoir l computed at $\omega = 0$, and

$$F_l(t - t') = \int \frac{d\varepsilon}{2\pi} \tanh \left[\frac{\beta_l}{2} (\varepsilon - \mu_l) \right] e^{-i\varepsilon t}. \quad (\text{A12})$$

APPENDIX B: SADDLE-POINT EQUATIONS

1. Variation of the action

Using the notation $\vec{\phi} = \{i\varrho_r(z), \phi\}$, we define classical and quantum fields as

$$\begin{pmatrix} \vec{\phi}_{c,r}^i(t') \\ \vec{\phi}_{q,r}^i(t') \end{pmatrix} = \frac{1}{\sqrt{2}} \begin{pmatrix} 1 & 1 \\ 1 & -1 \end{pmatrix} \begin{pmatrix} \vec{\phi}_r^i(t') \\ \overleftarrow{\phi}_r^i(t') \end{pmatrix}, \quad (\text{B1})$$

where $\vec{\phi}_r^i(t)$, $\overleftarrow{\phi}_r^i(t) = \vec{\phi}_r^i(z)$ (for $z \in \gamma_{\rightarrow}, \gamma_{\leftarrow}$) are, respectively, the Hubbard-Stratonovich fields in the forward and backward parts of the contour. In this way, we have that

$$\begin{aligned} & \sum_{r,i} \int_{\gamma} dz \pi_i^{-1} \vec{\phi}_r^i(z) \overleftarrow{\phi}_r^i(z) \\ &= \pi_i^{-1} \sum_{r,i} \int dt \begin{pmatrix} \vec{\phi}_r^i(t) \\ \overleftarrow{\phi}_r^i(t) \end{pmatrix}^T \begin{pmatrix} 1 & 0 \\ 0 & -1 \end{pmatrix} \begin{pmatrix} \vec{\phi}_r^i(t') \\ \overleftarrow{\phi}_r^i(t') \end{pmatrix} \\ &= \pi_i^{-1} \sum_{ri} \int dt \begin{pmatrix} \vec{\phi}_{c,r}^i(t) \\ \vec{\phi}_{q,r}^i(t) \end{pmatrix}^T \begin{pmatrix} 0 & 1 \\ 1 & 0 \end{pmatrix} \begin{pmatrix} \vec{\phi}_{c,r}^i(t') \\ \vec{\phi}_{q,r}^i(t') \end{pmatrix}. \end{aligned} \quad (\text{B2})$$

We proceed to find the saddle-point equations $\delta_{\phi_{i,r}(t)} S[\phi] = 0$, resulting in

$$\vec{\phi}_{c,r}^i(t) = \frac{i}{2} \pi_i \text{tr} \left[\frac{1}{\sqrt{2}} (G_{rr}^T(t, t^+) + G_{rr}^{\bar{T}}(t^+, t)) \sigma^i \right], \quad (\text{B3})$$

$$\vec{\phi}_{q,r}^i(t) = \frac{i}{2} \pi_i \text{tr} \left[\frac{1}{\sqrt{2}} (G_{rr}^T(t, t^+) - G_{rr}^{\bar{T}}(t^+, t)) \sigma^i \right], \quad (\text{B4})$$

with G^T and $G^{\bar{T}}$ being the propagators on the forward and backward parts of the contour. Evaluated at the causal solution $\vec{\phi}_{q,r}^i(t) = 0$, we obtain

$$\vec{\phi}_{c,r}^i(t) = \frac{i}{2} \pi_i \text{tr} \left[\frac{1}{\sqrt{2}} G_{rr}^K(t, t) \sigma^i \right] \quad (\text{B5})$$

2. Steady state

From Dyson's equation, i.e., $[G^{-1}]^{R/A} G^{R/A} = 1$, $[G^R]^{-1} G^K = \Sigma^K G^A$, and $G^K [G^A]^{-1} = G^R \Sigma^K$ (see, for

example, [71]), and with the steady-state values of the fields given by the parametrization in Eq. (3), we obtain

$$G^R(\omega) = (\omega - \mathbf{K})^{-1}, \quad (\text{B6})$$

where

$$\mathbf{K} = \mathbf{H} - i\Gamma, \quad (\text{B7})$$

with

$$\mathbf{H} = \sum_{rr'\sigma} |\mathbf{r}, s\rangle [-\tilde{t}_{r,r'} - \frac{1}{2} \delta_{rr'} \sigma_{ss'} \cdot \boldsymbol{\phi}_r - \mu_r] \langle \mathbf{r}', s'|, \quad (\text{B8})$$

$$\Gamma = \Gamma_L + \Gamma_R, \quad (\text{B9})$$

$$\Gamma_l = \Gamma_l |\mathbf{r}_l\rangle \langle \mathbf{r}_l|, \quad (\text{B10})$$

is a single-particle operator. With this notation, the many-body operator K defined in the main text is given by

$$K = \sum_{rr'ss'} c_{rs}^\dagger \langle \mathbf{r}s | \mathbf{K} | \mathbf{r}'s' \rangle c_{r's'}.$$

Assuming that \mathbf{K} is diagonalizable with right and left eigenvectors

$$\mathbf{K} |\alpha\rangle = \lambda_\alpha |\alpha\rangle, \quad (\text{B11})$$

$$\langle \tilde{\alpha} | \mathbf{K} = \lambda_\alpha \langle \tilde{\alpha} |, \quad (\text{B12})$$

such that $\text{Im} \lambda_\alpha < 0$, we can express it as

$$\mathbf{K} = \sum_{\alpha} |\alpha\rangle \lambda_\alpha \langle \tilde{\alpha}| \quad (\text{B13})$$

with the identities

$$\sum_{\alpha} |\alpha\rangle \langle \tilde{\alpha}| = \sum_{\alpha} |\tilde{\alpha}\rangle \langle \alpha| = 1, \quad (\text{B14})$$

$$\langle \alpha, | \tilde{\alpha}' \rangle = \delta_{\alpha\alpha'}. \quad (\text{B15})$$

With this notation, we can parametrize the Keldysh component of the Green's function as

$$G^K(\omega) = G^R(\omega) F(\omega) - F(\omega) G^A(\omega) \quad (\text{B16})$$

with

$$F(\omega) = \sum_{\alpha\alpha'} |\alpha\rangle \frac{-2i \sum_l \tanh \left[\frac{\beta_l}{2} (\omega - \mu_l) \right] \langle \tilde{\alpha} | \Gamma_l | \tilde{\alpha}' \rangle}{\lambda_\alpha - \bar{\lambda}_{\alpha'}} \langle \alpha' |.$$

APPENDIX C: STABILITY CONDITIONS AT $\phi = 0$

The second-order approximation of the action around $\phi \simeq 0$ is given by

$$\begin{aligned} S[\phi] &\simeq \frac{1}{2} [\phi \pi^{-1} \phi] - i \left\{ \text{tr} \ln [-i(G_0^{-1})] - \frac{1}{2} \text{tr} [(G_0 \Sigma)^2] \right\} \\ &= -i \text{tr} \ln [-i(G_0^{-1})] + \frac{1}{2} \sum_{rr'} \int \frac{d\omega}{2\pi} \begin{pmatrix} \phi_{c,r}^i(t) \\ \phi_{q,r}^i(t) \end{pmatrix}^T \\ &\quad \times \begin{pmatrix} 0 & [\chi^{-1}]_{i,jrr'}^A(t, t') \\ [\chi^{-1}]_{i,jrr'}^R(t, t') & [\chi^{-1}]_{i,jrr'}^K(t, t') \end{pmatrix} \begin{pmatrix} \phi_{c,r}^i(t') \\ \phi_{q,r}^i(t') \end{pmatrix} \end{aligned} \quad (\text{C1})$$

with $G_0^{-1} = G^{-1}|_{\phi=0}$. The magnetic susceptibility is defined as $\chi_{rr'}^{ij}(z, z') = -i \langle T_\gamma S_r^i(z) S_{r'}^j(z') \rangle$. Explicitly, we have

$$[X^{-1}]_{rr'}^{ij}(t, t') = \delta_{ij} \begin{pmatrix} 0 & -\frac{3}{2U} \delta_{rr'} \delta(t - t') - \frac{1}{2} \Xi_{ij;rr'}^A(t, t') \\ -\frac{3}{2U} \delta_{rr'} \delta(t - t') - \frac{1}{2} \Xi_{ij;rr'}^R(t, t') & -\frac{1}{2} \Xi_{ij;rr'}^K(t, t') \end{pmatrix},$$

where Ξ denotes the bubblelike diagrams

$$\begin{aligned} \Xi_{rr'}^{R/A}(t, t') &= -i \frac{1}{2} \text{tr} [G_{0;rr'}^{A/R}(t', t) G_{0;rr'}^K(t, t') + G_{0;rr'}^K(t', t) G_{0;rr'}^{R/A}(t, t')], \\ \Xi_{rr'}^K(t, t') &= -i \frac{1}{2} \text{tr} [G_{0;rr'}^A(t', t) G_{0;rr'}^R(t, t') + G_{0;rr'}^R(t', t) G_{0;rr'}^A(t, t') + G_{0;rr'}^K(t', t) G_{0;rr'}^K(t, t')]. \end{aligned}$$

Assuming a steady-state condition, we obtain, for the retarded component,

$$\begin{aligned} \Xi_{rr'}^R(\omega) &= \Xi_{rr'}^{(1)}(\omega) + \bar{\Xi}_{rr'}^{(2)}(-\omega) + \Xi_{rr'}^{(2)}(\omega) + \bar{\Xi}_{rr'}^{(1)}(-\omega), \\ \Xi_{rr'}^{(1)}(\omega) &= - \sum_{\alpha\beta} \sum_l \langle r' | \tilde{\beta} \rangle \langle \beta | r \rangle \langle r | \alpha \rangle A_{\alpha r'}^l I_l(\bar{\lambda}_\beta + \omega, \lambda_\alpha), \\ \Xi_{rr'}^{(2)}(\omega) &= - \sum_{\alpha\beta} \sum_l \langle r' | \alpha \rangle \langle r | \beta \rangle \langle \tilde{\beta} | r' \rangle A_{\alpha r'}^l I_l(\lambda_\beta - \omega, \lambda_\alpha), \end{aligned}$$

with

$$I_l(z, z') = \frac{1}{\pi} \frac{\psi^{(0)}\left[\frac{1}{2} - i \text{sgn}(\text{Im}z') \frac{\beta_l(z' - \mu_l)}{2\pi}\right] - \psi^{(0)}\left[\frac{1}{2} - i \text{sgn}(\text{Im}z) \frac{\beta_l(z - \mu_l)}{2\pi}\right]}{z - y}, \quad A_{\alpha r'}^l = \sum_{\alpha'} \frac{\langle \tilde{\alpha} | \Gamma_l | \tilde{\alpha}' \rangle \langle \alpha' | r \rangle}{\lambda_\alpha - \bar{\lambda}_{\alpha'}},$$

and $\psi^{(0)}(z) = \partial_z \ln \Gamma(z)$ is the logarithmic derivative of the Γ function.

APPENDIX D: SUPPLEMENTAL NUMERICAL RESULTS

1. Discussion of finite-size effects

Mean-field arguments are expected to be more accurate in the weak-coupling limit for small values of U . In the main text, we illustrate our findings with numerical results obtained for $U = 6.2$. Even if $U = 6.2$ corresponds to a rather small ratio $U/W \simeq 1.55$ (with W the bandwidth), it already belongs to the crossover region between weak and strong coupling. In this Appendix, we justify our choice of U values due to the appearance of strong finite-size effects for small U .

Figure 4 shows the mean-field phase diagram for different values of the hybridization Γ and for different system sizes

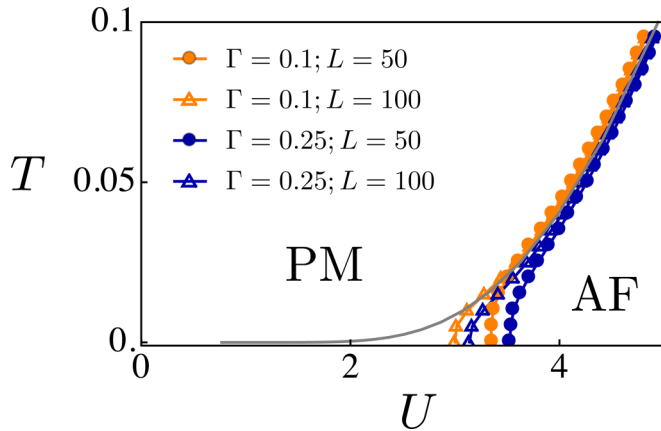


FIG. 4. Behavior of finite-size effects for $V = 0$. The mean-field transition temperature, separating the paramagnetic (PM) from the antiferromagnetic (AF) phases, is computed for two different values of the hybridization Γ and for different system sizes L (colored symbols). The infinite-size result is depicted by the gray line.

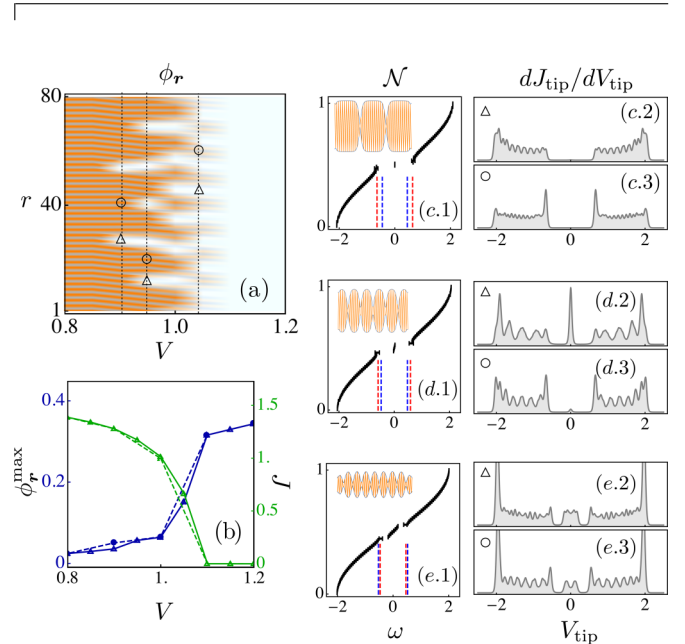


FIG. 5. Properties for $U > U_c$ obtained for $\Gamma = 0.25$, $T = 0.25$, and $U = 8.55$ corresponding to an equilibrium ($V = 0$) charge gap of $\Delta = 2|\phi| \simeq 3.2$. (a) Density plot of $\Phi(r)$ plotted as a function of V for $L = 80$. The lines and markers label the specific values of (c)–(e). (b) Maximum value of the order parameter $\phi_{\text{Max}} = \max_r |\phi(r)|$ (green) and particle current through the chain J (blue) as a function of V for $L = 80$ (open triangles) and $L = 120$ (full circles). (c.1) Integrated density of states $\mathcal{N}(\omega) = \sum_{\alpha} \Theta(\omega - \text{Re}\lambda_{\alpha})$ for $V = 0.9$ and $L = 80$; the thickness of the black line is given by $\text{Im}\lambda_{\alpha}$. The red-dashed lines correspond to $\omega = \pm \phi_{\text{Max}}$ and the blue-dashed lines to $\omega = \pm V/2$. The inset depicts the spatial dependence of $\phi(r)$. (c.2), (c.3) Differential conductance $dJ_{\text{tip}}/dV_{\text{tip}}$ obtained by an STM tip, computed for $T_{\text{tip}} = 0.02$, placed at position r , for $r = 27$ (c.2) and $r = 41$ (c.3), corresponding to a minimum and a maximum of the order-parameter amplitude. (d.1)–(d.3) Same as (c.1)–(c.3) for $V = 0.95$, $r = 12$, and $r = 19$. (e.1)–(e.3) Same as (c.1)–(c.3) for $V = 1.05$, $r = 45$, and $r = 59$.

L computed for $V = 0$. Compared with the infinite-size limit, there are strong finite-size corrections arising for small U for which the paramagnetic phase extends up to zero temperature.

As the numerical results are obtained by solving the self-consistent equations for the order parameter in real space, the computation times scale with the system size. To ensure that the reported finite-size effects do not affect the results, in the range of considered systems sizes ($L \simeq 50, 80, 100$), $U = 6.2$ was chosen as a compromise.

2. Nonlinear regime, $U = 8.55$

The main text shows results for the intermediate-coupling regime, corresponding to values of U of the order of the

bandwidth. From the phase diagram of Fig. 2, obtained by analyzing the susceptibility, the small-to-intermediate U requirement implies that the pair (V_c, T) , with V_c defined as $U_c(T, V_c) = U$, belongs either to region I or II. In case it belongs to region I, the scenario of the phase transition is similar to the equilibrium one and no pattern formation arises. The nontrivial case arises for $(V_c, T) \in \text{II}$, studied in the main text. In this case, to show that our results are robust to the particular choice of U , we provide additional numerical results to those of the main text, here obtained for $U = 8.55$ and depicted in Fig. 5. Note that Fig. 5 shows the same characteristic features for the $U = 6.3$ case; see the discussion in the main text.

-
- [1] M. Cross and P. Hohenberg, *Rev. Mod. Phys.* **65**, 851 (1993).
- [2] G. Nicolis and I. Prigogine, *Self-organization in Nonequilibrium Systems: From Dissipative Structures to Order through Fluctuations* (Wiley, New York, 1977).
- [3] P. Ball, *The Self-Made Tapestry: Pattern Formation in Nature* (Oxford University Press, Oxford, 1999).
- [4] E. Schöll, *Nonequilibrium Phase Transitions in Semiconductors*, Springer Series in Synergetics Vol. 35 (Springer, Berlin, 1987).
- [5] R. Kumai, *Science* **284**, 1645 (1999).
- [6] J. Kronjäger, C. Becker, P. Soltan-Panahi, K. Bongs, and K. Sengstock, *Phys. Rev. Lett.* **105**, 090402 (2010).
- [7] M. O. Borgh, J. Keeling, and N. G. Berloff, *Phys. Rev. B* **81**, 235302 (2010).
- [8] N. G. Berloff and J. Keeling, *Physics of Quantum Fluids*, Springer Series in Solid-State Sciences Vol. 177 (Springer, Berlin, 2013).
- [9] I. Bloch and W. Zwerger, *Rev. Mod. Phys.* **80**, 885 (2008).
- [10] N. Strohmaier, D. Greif, R. Jördens, L. Tarruell, H. Moritz, T. Esslinger, R. Sensarma, D. Pekker, E. Altman, and E. Demler, *Phys. Rev. Lett.* **104**, 080401 (2010).
- [11] T. Langen, R. Geiger, and J. Schmiedmayer, *Annu. Rev. Condens. Matter Phys.* **6**, 201 (2015).
- [12] A. Cavalleri, C. Tóth, C. Siders, J. Squier, F. Ráksi, P. Forget, and J. Kieffer, *Phys. Rev. Lett.* **87**, 237401 (2001).
- [13] F. Novelli, G. De Filippis, V. Cataudella, M. Esposito, I. Vergara, F. Cilento, E. Sindici, A. Amaricci, C. Giannetti, D. Prabhakaran, S. Wall, A. Perucchi, S. Dal Conte, G. Cerullo, M. Capone, A. Mishchenko, M. Grüninger, N. Nagaosa, F. Parmigiani, and D. Fausti, *Nat. Commun.* **5**, 5112 (2014).
- [14] M. Rigol, V. Dunjko, and M. Olshanii, *Nature (London)* **452**, 854 (2008).
- [15] M. Srednicki, *Phys. Rev. E* **50**, 888 (1994).
- [16] J. Deutsch, *Phys. Rev. A* **43**, 2046 (1991).
- [17] J. Eisert, M. Friesdorf, and C. Gogolin, *Nat. Phys.* **11**, 124 (2015).
- [18] S. Diehl, A. Micheli, A. Kantian, B. Kraus, H. P. Büchler, and P. Zoller, *Nat. Phys.* **4**, 878 (2008).
- [19] S. Diehl, A. Tomadin, A. Micheli, R. Fazio, and P. Zoller, *Phys. Rev. Lett.* **105**, 015702 (2010).
- [20] L. M. Sieberer, S. D. Huber, E. Altman, and S. Diehl, *Phys. Rev. Lett.* **110**, 195301 (2013).
- [21] A. Mitra, S. Takei, Y. Kim, and A. Millis, *Phys. Rev. Lett.* **97**, 236808 (2006).
- [22] A. Mitra and A. Millis, *Phys. Rev. B* **77**, 220404 (2008).
- [23] S. Takei, W. Witczak-Krempa, and Y. B. Kim, *Phys. Rev. B* **81**, 125430 (2010).
- [24] C. H. Chung, K. Le Hur, M. Vojta, and P. Wölfle, *Phys. Rev. Lett.* **102**, 216803 (2009).
- [25] S. Kirchner and Q. Si, *Phys. Rev. Lett.* **103**, 206401 (2009).
- [26] P. Ribeiro, Q. Si, and S. Kirchner, *Europhys. Lett.* **102**, 50001 (2013).
- [27] P. Werner, T. Oka, and A. Millis, *Phys. Rev. B* **79**, 035320 (2009).
- [28] M. Schiró and M. Fabrizio, *Phys. Rev. B* **79**, 153302 (2009).
- [29] E. Gull, D. R. Reichman, and A. J. Millis, *Phys. Rev. B* **82**, 075109 (2010).
- [30] E. Gull, D. R. Reichman, and A. J. Millis, *Phys. Rev. B* **84**, 085134 (2011).
- [31] G. Cohen, E. Gull, D. R. Reichman, A. J. Millis, and E. Rabani, *Phys. Rev. B* **87**, 195108 (2013).
- [32] H. Aoki, N. Tsuji, M. Eckstein, M. Kollar, T. Oka, and P. Werner, *Rev. Mod. Phys.* **86**, 779 (2014).
- [33] M. Schiró and M. Fabrizio, *Phys. Rev. Lett.* **105**, 076401 (2010).
- [34] M. Schiró and M. Fabrizio, *Phys. Rev. B* **83**, 165105 (2011).
- [35] S. Okamoto, *Phys. Rev. B* **76**, 035105 (2007).
- [36] S. Okamoto, *Phys. Rev. Lett.* **101**, 116807 (2008).
- [37] M. Eckstein, A. Hackl, S. Kehrein, M. Kollar, M. Moeckel, P. Werner, and F. Wolf, *Eur. Phys. J. Spec. Top.* **180**, 217 (2010).
- [38] M. Knap, W. von der Linden, and E. Arrighoni, *Phys. Rev. B* **84**, 115145 (2011).
- [39] A. Amaricci, C. Weber, M. Capone, and G. Kotliar, *Phys. Rev. B* **86**, 085110 (2012).
- [40] C. Aron, G. Kotliar, and C. Weber, *Phys. Rev. Lett.* **108**, 086401 (2012).
- [41] E. Arrighoni, M. Knap, and W. von der Linden, *Phys. Rev. Lett.* **110**, 086403 (2013).
- [42] G. Mazza, A. Amaricci, M. Capone, and M. Fabrizio, *Phys. Rev. B* **91**, 195124 (2015).
- [43] M. Moeckel and S. Kehrein, *Phys. Rev. Lett.* **100**, 175702 (2008).
- [44] M. Eckstein, M. Kollar, and P. Werner, *Phys. Rev. Lett.* **103**, 056403 (2009).
- [45] T. Enss and J. Sirker, *New J. Phys.* **14**, 023008 (2012).

- [46] C. Karrasch, D. M. Kennes, and J. E. Moore, *Phys. Rev. B* **90**, 155104 (2014).
- [47] T. Prosen and M. Žnidarič, *Phys. Rev. B* **86**, 125118 (2012).
- [48] T. Prosen, *Phys. Rev. Lett.* **112**, 030603 (2014).
- [49] J. E. Han and J. Li, *Phys. Rev. B* **88**, 075113 (2013).
- [50] P. Ribeiro and V. R. Vieira, *Phys. Rev. B* **92**, 100302 (2015).
- [51] T. Oka, R. Arita, and H. Aoki, *Phys. Rev. Lett.* **91**, 066406 (2003).
- [52] T. Oka and H. Aoki, *Phys. Rev. Lett.* **95**, 137601 (2005).
- [53] M. Eckstein, T. Oka, and P. Werner, *Phys. Rev. Lett.* **105**, 146404 (2010).
- [54] M. Eckstein and P. Werner, *Phys. Rev. Lett.* **107**, 186406 (2011).
- [55] J. Li, C. Aron, G. Kotliar, and J. E. Han, *Phys. Rev. Lett.* **114**, 226403 (2015).
- [56] J. Neumayer, E. Arrighi, M. Aichhorn, and W. von der Linden, *Phys. Rev. B* **92**, 125149 (2015).
- [57] W. R. Lee and K. Park, *Phys. Rev. B* **89**, 205126 (2014).
- [58] Z. Lenarčič and P. Prelovšek, *Phys. Rev. Lett.* **108**, 196401 (2012).
- [59] M. Mierzejewski, J. Bonča, and P. Prelovšek, *Phys. Rev. Lett.* **107**, 126601 (2011).
- [60] Y. Taguchi, T. Matsumoto, and Y. Tokura, *Phys. Rev. B* **62**, 7015 (2000).
- [61] C. Vaju, L. Cario, B. Corraze, E. Janod, V. Dubost, T. Cren, D. Roditchev, D. Braithwaite, and O. Chauvet, *Adv. Mater.* **20**, 2760 (2008).
- [62] V. Guiot, L. Cario, E. Janod, B. Corraze, V. Ta Phuoc, M. Rozenberg, P. Stoliar, T. Cren, and D. Roditchev, *Nat. Commun.* **4**, 1722 (2013).
- [63] N. Sugimoto, S. Onoda, and N. Nagaosa, *Phys. Rev. B* **78**, 155104 (2008).
- [64] Y. Tanaka and K. Yonemitsu, *Phys. Rev. B* **83**, 085113 (2011).
- [65] F. Heidrich-Meisner, I. González, K. A. Al-Hassanieh, A. E. Feiguin, M. J. Rozenberg, and E. Dagotto, *Phys. Rev. B* **82**, 205110 (2010).
- [66] A. Gomes and P. Lederer, *J. Phys.* **38**, 231 (1977).
- [67] G. Stefanucci, *Phys. Rev. B* **75**, 195115 (2007).
- [68] F. Heidrich-Meisner, A. E. Feiguin, and E. Dagotto, *Phys. Rev. B* **79**, 235336 (2009).
- [69] P. Werner, T. Oka, M. Eckstein, and A. J. Millis, *Phys. Rev. B* **81**, 035108 (2010).
- [70] A. E. Antipov, Q. Dong, and E. Gull, *Phys. Rev. Lett.* **116**, 036801 (2016).
- [71] J. Maciejko, *An Introduction to Nonequilibrium Many-Body Theory* (Springer, 2007).